The Cryosphere Discuss., 9, 2259–2299, 2015
www.the-cryosphere-discuss.net/9/2259/2015/
doi:10.5194/tcd-9-2259-2015

The Cryosphere Discussions
Open Access

Impact of debris cover on glacier ablation and atmosphere-glacier feedbacks in the Karakoram

E. Collier[1,2], **F. Maussion**[3], **L. I. Nicholson**[3], **T. Mölg**[4], **W. W. Immerzeel**[1], **and A. B. G. Bush**[2]

[1]Faculty of Geosciences, Utrecht University, Utrecht, the Netherlands
[2]Department of Earth and Atmospheric Sciences, University of Alberta, Edmonton, Canada
[3]Institute of Meteorology and Geophysics, University of Innsbruck, Innsbruck, Austria
[4]Climate System Research Group, Institute of Geography, Friedrich-Alexander-University Erlangen-Nürnberg (FAU), Germany

Received: 1 March 2015 – Accepted: 10 March 2015 – Published: 8 April 2015

Correspondence to: E. Collier (eec@ualberta.ca)

Published by Copernicus Publications on behalf of the European Geosciences Union.

Abstract

The Karakoram range of the Hindu-Kush-Himalaya is characterized by both extensive glaciation and a widespread prevalence of surficial debris cover on the glaciers. Surface debris exerts a strong control on glacier surface-energy and mass fluxes and, by modifying surface boundary conditions, has the potential to alter atmosphere-glacier feedbacks. To date, the influence of debris on Karakoram glaciers has only been directly assessed by a small number of glaciological measurements over short periods. Here, we include supraglacial debris in a high-resolution, interactively coupled atmosphere-glacier modelling system. To investigate glaciological and meteorological changes that arise due to the presence of debris, we perform two simulations using the coupled model from 1 May to 1 October 2004: one that treats all glacier surfaces as debris-free and one that introduces an simplified specification for mapping debris thickness. The basin-averaged impact of debris is a reduction in ablation of $\sim 7\,\%$, although the difference exceeds 2.5 m w.e. on the lowest-altitude glacier tongues. The modest reduction in mean mass loss results in part from non-negligible sub-debris melt rates under thicker covers and from compensating increases in melt under thinner debris, and may help to explain the lack of distinct differences in recent elevations changes between clean and debris-covered ice. The presence of debris also strongly alters the surface boundary condition and thus heat exchanges with the atmosphere; near-surface meteorological fields at lower elevations and their vertical gradients; and the atmospheric boundary layer development. These findings are relevant for glacio-hydrological studies on debris-covered glaciers and contribute towards an improved understanding of glacier behaviour in the Karakoram.

TCD
9, 2259–2299, 2015

1 Introduction

The Karakoram region of the greater Himalaya (~ 74–77° E, 34–37° N; Fig. 1) is extensively glaciated, with an ice-covered area of ~ 18 000 km^2 (Bolch et al., 2012). Supraglacial debris is widespread, and covers an estimated ~ 18–22 % of the glacierized area (Scherler et al., 2011; Hewitt, 2011), which is approximately twice as large as the Himalayan average of ~ 10 % (Bolch et al., 2012). The region has received a great deal of public and scientific attention in recent years due to evidence of stable or even slightly positive mass balances in the 2000s (Hewitt, 2005; Scherler et al., 2011; Gardelle et al., 2012, 2013; Kääb et al., 2012) that are in contrast with predominantly negative balances of glaciers in the rest of the Hindu-Kush-Himalaya (HKH; Cogley, 2011) Knowledge of the hydrological response of Karakoram glaciers to climate change is critical, since their meltwater contributes to freshwater resources in the highly populated region of South Asia (Kaser et al., 2010; Lutz et al., 2014). However, due to logistical constraints and political instability, field observations of glaciological and meteorological conditions in the Karakoram are sparse in space and time, in particular at high altitudes (Mihalcea et al., 2006, 2008; Mayer et al., 2014). Although observational records have been supplemented in recent decades by remote sensing data (e.g. Gardelle et al., 2012, 2013; Kääb et al., 2012), large gaps remain in our understanding of the important drivers of glacier change in this region, including regional atmospheric conditions, local topography and glacier debris cover, as well as interactions between them. Physically based numerical modelling has the potential to supplement observations and provide additional insight into contemporary glacier dynamics as well as to provide a methodology for predictions of future glacier response.

The prevalence of debris cover has a strong potential influence on glacier behaviour in the Karakoram, as field studies have shown that debris cover can significantly alter the ice ablation rate compared to that of clean ice (e.g. Østrem, 1959; Fujii, 1977; Inoue and Yoshida, 1980). Ice melt is enhanced beneath debris cover less than a few centimeters thick due to increased absorption of solar radiation, and ice ablation decreases

TCD
9, 2259–2299, 2015

exponentially with increasing thickness due to insulation of the ice from atmospheric energy sources. Surficial debris also drastically alters glacier surface conditions, by permitting surface temperature to exceed the melting point and by modifying the surface roughness and saturation conditions, which impacts the surface energy fluxes (Inoue and Yoshida, 1980; Takeuchi et al., 2001; Brock et al., 2010) and the atmospheric boundary layer (Granger et al., 2002). Therefore, there is a strong potential for debris-covered ice to affect atmosphere-glacier feedbacks in this region.

Two main issues arise in attempting to include the influence of debris cover in simulations of Karakoram glaciers. First, the debris thickness, extent and thermal properties are largely unknown and their specification is highly uncertain. Second, the spatial distribution of meteorological forcing data is complicated by highly heterogeneous surface conditions in the ablation zone (e.g. Nicholson and Benn, 2012) and the complex topography, with current approaches that use elevation-based extrapolation appearing to be inadequate (Reid et al., 2012). Here, we investigate the influence of debris cover on Karakoram glacier surface-energy and mass exchanges and feedbacks with the atmosphere over an ablation season, using an interactively coupled atmosphere and glacier climatic mass balance (CMB) model that includes debris cover. By comparing a debris free simulation to a simulation where we include debris cover with a simple specification of thickness, we first quantify differences in the surface energy balance and mass fluxes. We then assess (1) feedbacks between the atmosphere and glacier surfaces using the coupled model and (2) differences in boundary layer development and turbulent fluxes.

2 Methods

The modelling tool employed in this study is the interactively coupled, high-resolution, regional atmosphere and glacier climatic mass balance model WRF-CMB, which explicitly resolves the surface-energy and CMB processes of alpine glaciers at the regional scale (Collier et al., 2013). The coupled model has been previously applied to

TCD
9, 2259–2299, 2015

the study region neglecting debris cover and was capable of reproducing the magnitudes of the few available observations of glacier CMB in this region. The changes introduced to the atmospheric and glacier CMB model components for this study are described in Sects. 2.1 and 2.2, respectively. Using WRF-CMB, we performed two simulations for the period of 1 April to 1 October 2004: the first treated all glacier surfaces as debris-free (*CLN*) and the second introduced an simplified debris thickness specification (*DEB*), which is described in Sect. 2.3.

2.1 Regional atmospheric model

The atmospheric component of WRF-CMB is the Advanced Research version of the Weather Research and Forecasting (WRF) model version 3.6.1 (Skamarock and Klemp, 2008). In this study, WRF was configured with three nested domains, of 30, 10, and 2 km resolution, which were centered over the Karakoram region (Fig. 1). The domains had 40 vertical levels, with the model top located at 50 hPa. The model configuration was based on the previous application of WRF-CMB over this region (Collier et al., 2013, Table 1). However, for this study, the land surface model was updated to the Noah-MP scheme (Niu et al., 2011), which provides an improved treatment of snow physics in non-glaciated grid cells compared with the Noah scheme (Chen and Dudhia, 2001) that was previously used, by prognosing the energy balance and skin temperature of the vegetation canopy and snowpack separately, introducing multiple layers in the snowpack, and providing an improved treatment of frozen soils. Note that the prognosis of surface and subsurface conditions for glaciated grid cells is performed by the CMB model, which is discussed in the next section. The adaptive time stepping scheme was used, which greatly increased the execution speed of the simulations. Horizontal diffusion was also changed to be computed in physical space rather than along model levels, since this option is recommended by WRF developers for applications in complex terrain, where the vertical levels are significantly sloped. Finally, for the finest-resolution domain (hereafter WRF D3), slope effects on radiation and topographic shading were accounted for and a cumulus parameterization was neglected,

TCD
9, 2259–2299, 2015

since at 2 km resolution, it is assumed to be convection permitting (e.g. Molinari and Dudek, 1992; Weisman et al., 1997).

The USGS land cover data used by WRF was updated to incorporate more recent glacier inventories for the region. Over the Himalayan region, we used the glacier outlines from the Randolph Glacier Inventory v. 3.2 (Pfeffer et al., 2014). For the Karakoram itself, we used the inventory of Rankl et al. (2014), which was obtained by updating the RGI manually on the basis of Landsat scenes. To determine which grid cells in each WRF domain were glaciated, the outlines were rasterized on a high-resolution grid that was 50-times higher than the original grid spacing of the domain. The fractional glacier coverage of grid cells in each domain was calculated on this finer grid, and a threshold of 40 % coverage was used to classify a grid cell as "glacier." The soil categories and vegetation parameters were updated to be consistent with the glacier outlines.

The atmospheric model was forced at the boundaries of the coarse-resolution domain with the ERA-Interim reanalysis from the European Centre for Medium-Range Weather Forecasts (ECMWF; Dee et al., 2011). The spatial and temporal resolution of the ERA-Interim data are approximately 80 km (T255 spectral resolution) and 6 hourly, respectively. Snow depths in ERA Interim over the Karakoram are unrealistic (more than 20 m Collier et al., 2013), therefore an alternative initial snow condition was provided by the Global EASE-Grid 8 day blended SSM/I and MODIS snow cover dataset for snow water equivalent (Brodzik et al., 2007), by assuming a snow density of 300 $kg\,m^{-3}$ and specifying a depth of 0.5 m for areas with missing data, such as over large glaciers. This assumption affected 0.7, 5 and 40 % of grid points in D1–D3, respectively.

2.2 Glacier CMB model with debris treatment

The original basis of the glacier CMB model is the physically based model of (Mölg et al., 2008, 2009). The model solves the full energy balance equation to determine the energy for snow and ice ablation. The computation of the total column mass balance accounts for: surface and sub-surface melt, refreeze and changes in liquid water

TCD
9, 2259–2299, 2015

storage in the snowpack, surface vapor fluxes, and solid precipitation. The CMB model was adapted for interactive coupling with WRF by Collier et al. (2013) and modified to include supraglacial debris by Collier et al. (2014). For the version employed in this study, a time-varying snowpack is introduced on top of a static debris layer, both of which overly a column of ice resolved down to a depth of 7.0 m. The vertical levels in the subsurface used for these simulations are presented in Table 2.

The CMB model is a key component of this study, since it not only provides a treatment of debris cover but also permits snow-free conditions on glaciers, whereas the Noah-MP LSM imposes a minimum snow depth of 0.1 m w.e. For these simulations, debris cover is introduced in the finest-resolution domain only, since it provides the best representation of both the complex topography and glacier extents.

A full description of the debris modifications is given by Collier et al. (2014), however we provide a brief summary here. The debris layer is resolved into 1 cm layers and has an assumed porosity function that decreases linearly with depth. The properties of each layer in the debris are computed as weighted functions of whole-rock values and the contents of the pore space (air, water or ice) using values presented in Table 3. For the whole-rock values, the albedo was based on 50 spot measurements on a debris-covered glacier in Nepal (Nicholson and Benn, 2012); the density and thermal conductivity were selected as representative values spanning major rock types taken from Daly et al. (1966); Clark (1966), respectively; and, the specific heat capacity was taken from Conway and Rasmussen (2000). Moisture in the debris and its phase are modelled using a simple reservoir parameterization. When debris is exposed at the surface, the surface vapor pressure is parameterized as a simple linear function of the debris water and ice content.

Surface temperature is predicted using an iterative approach to determine the value that yields zero net flux in the surface energy balance equation. Initial test simulations with WRF-CMB over the Karakoram gave unrealistically cold surface temperatures as a result of excessive nighttime damping of the turbulent fluxes, in particular the sensible heat flux (QS) over debris-free glacier surfaces at high elevations. The stability

TCD
9, 2259–2299, 2015

corrections are based on the bulk Richardson number (specifically, those provided in Braithwaite, 1995) and have been used previously in glacier CMB modelling (e.g. Mölg et al., 2008, 2009; Reid et al., 2012). In the most stable conditions, the turbulent fluxes are fully damped, which resulted in decoupling of the surface and the atmosphere and excessive radiative cooling. Even in less strongly stable conditions, the damping of modelled turbulent fluxes has been found to be excessive in comparison with eddy covariance measurements over glaciers (Conway and Cullen, 2013). To prevent decoupling in WRF-CMB, we introduced a minimum windspeed of $1\,m\,s^{-1}$, consistent with previous modelling studies of glacier surface energy fluxes (Martin and Lejeune, 1998) and with the Noah-MP LSM (Niu et al., 2011). Furthermore, we limit the maximum amount of damping to 30 % (Martin and Lejeune, 1998; Giesen et al., 2009).

To prevent errors arising from blended snow and debris layers, such as constraints on possible temperature solutions or excess melting, an adaptive vertical grid in the snowpack was introduced. For snow depths of up to one meter, the nearest integer number of 10 cm layers are assigned, while areas of the snowpack that exceed one meter are resolved into the nearest integer number of 50 cm layers. Snow depths between 1 and 10 cm are assigned a single computational layer, and depths less than 1 cm are not treated with a unique layer. Over regions of the snowpack where the layer depths have changed, normalized linear interpolation is performed to calculate temperature changes. This procedure conserves the bulk heat content of the snowpack, except when the depth crosses the minimum threshold of 1 cm. In both simulations, timestep changes in the bulk heat content of the snowpack in WRF D3 were small (less than 0.01 K). The CMB model is not designed for detailed snowpack studies and therefore only prognoses a bulk snow density. Since the total snow depth is not modified by the interpolation scheme, snow mass is conserved.

The debris-free version of the CMB model normally has levels located at fixed depths in the subsurface, with the thermal and physical properties of each layer computed as a weighted average of the snow and ice content. However, to isolate the influence of debris on glacier energy and mass fluxes, the CLN simulation also employs the adap-

TCD
9, 2259–2299, 2015

tive vertical grid in the snowpack in this study. A test simulation from 1 April to 15 May 2004 was performed to compare the two adapative and non-adaptive grid, with reasonable agreement in simulated snow depth (R^2 = 0.99; mean deviation, MD = −1.9 cm) and snow melt (R^2 = 0.87; MD = 6.8×10^{-4} kg m^{-2}).

2.3 Specification of debris extent and thickness in WRF D3

The RGI and the inventory of Rankl et al. (2014) provide glacier outlines that include debris-covered glacier areas when detected, but they do not delineate these areas. To define debris-covered areas in WRF D3, the clean ice/firn/snow mask of Kääb et al. (2012) was rasterized on the same high-resolution (40 m) grid used to compute glaciated grid cells (cf. Sect. 2.1). For each WRF pixel, the percent coverage of debris was determined and the same threshold of 40 % was used to classify a glacier pixel as debris-covered. Figure 2a provides an example of the delineation for the Baltoro glacier 76° 26′ E, 35° 45′ N). We note that any debris-covered glacier areas that are not detected during the generation of the glacier outlines are missed.

Specifying the debris thickness was more complex, since this field varies strongly over small spatial scales. For example, Nicholson and Benn (2012) reported very heterogeneous debris thickness varying between 0.5 and 2.0 m over distances of less than 100 m on the Ngozumpa glacier, Nepal. Spatial variability arises from many factors, including hillslope fluxes to the glacier; surface and subsurface transport; and, the presence of ice cliffs, melt ponds and crevasses (e.g. Brock et al., 2010; Zhang et al., 2011). The few available field measurements do not support a relationship between debris thickness and elevation (e.g. Mihalcea et al., 2006; Reid et al., 2012). However, measurements on the Tibetan plateau (Zhang et al., 2011), in Nepal (Nicholson and Benn, 2012), and in the Karakoram (Mihalcea et al., 2008) indicate that thicker values are more prevalent near glacier termini while thinner ones are more ubiquitous up-glacier.

In this study, we adopt an simple linear approach that was informed by this observed relationship to specify debris thickness over the areas identified as debris-covered in

TCD
9, 2259–2299, 2015

WRF D3. For this method, distance down-glacier was computed starting from the top of the debris-covered area of each glacier and moving along its centreline (Fig. 2b and d). Centerline data were provided by Rankl et al. (2014) for both main glacier trunks and their tributaries. We then assumed a fixed gradient to distribute debris over areas identified as being debris covered as a function of distance down glacier, with a single thickness specified in each 2 km grid cell. We tested two gradients, 1.0 and 0.75 cm km^{-1}, which gave thicknesses exceeding 40 and 30 cm, respectively, at the termini of the longest glaciers in the Karakoram (Fig. 2d). Where centerline information was unavailable (a region delineated by the red contour in Fig. 2d), a constant thickness of 10 cm was assigned to each debris-covered pixel. For clarity, these data are not included in Fig. 2c.

Both gradients are consistent with the ASTER-derived debris-thickness data for the Baltoro glacier of Mihalcea et al. (2008) after averaging onto the WRF D3 grid. However, these data show a non-linear increase close to the terminus, and indicate that the 1 cm km^{-1} gradient distributes too much debris in the middle ablation zone, while the 0.75 cm km^{-1} value distributes too little near the terminus. Here, we focus our discussion on the 0.75 cm km^{-1} gradient simulation and suggest that our analysis thus represents a conservative estimate of the impact of debris. However, since the non-linear increase is located close to the terminus, we assume the lower gradient is most valid at the regional scale. For comparison, the 1 cm km^{-1} gradient decreases the basin-mean mass loss between 1 July and 1 October by a further $\sim$ 7 % compared with the lower value.

This approach underestimates peak thicknesses at the termini of the Baltoro, which exceed 1 m (e.g. Mihalcea et al., 2008). However, it is well established that ablation decreases exponentially with debris thicknesses above a few centimeters (e.g. Østrem, 1959; Loomis, 1970; Mattson et al., 1993). As the debris layer is resolved into 1 cm layers, including debris depths of up to 1 m would therefore greatly increase the computational expense of the CMB model, with likely only a small change to the amount of sub-debris ice melt. In addition, features such as meltwater ponds and ice cliffs in the

TCD
9, 2259–2299, 2015

ablation zone absorb significantly more energy than adjacent debris-covered surfaces. These features may give compensatory high-melt rates (e.g. Inoue and Yoshida, 1980; Sakai et al., 1998, 2000; Pellicciotti et al., 2015; Immerzeel et al., 2014a) that support using a thinner average or "effective" debris thickness when assigning an average value to each 2 km grid cell in WRF-D3.

After applying this method, WRF D3 contains a total of 5273 glaciated grid cells, 821 of which are debris-covered glacier cells, which gives a proportion of debris-covered glacier area in WRF D3 of ∼ 16 %.

3 Results

3.1 Land surface temperature

For model evaluation, we compared simulated daytime LST with daily fields from the MODIS Terra MOD11A1 and Aqua MYD11A1 datasets at a spatial resolution of 1 km. Only MODIS data with the highest quality flag were used for the comparison and WRF-CMB data were taken from the closest available time step in local solar time. We focussed on daytime LST, because this field had a higher number of valid pixels at lower elevations over the simulation period than nighttime LST. Figure 3a shows mean elevational profiles of LST over glaciated pixels for composite MODIS data and for the CLN and DEB simulations. Although the modelled profiles are significantly colder than the MODIS data, the simulated profile in DEB is in much closer agreement than CLN, as LST exceeds the melting point below the simulated mean snow line at ∼ 4500 m a.s.l.

Examination of the MODIS LST data suggests that they may contain a warm bias, as a result of blending of different glacier surface types as well as glaciated and non-glaciated areas on the 1 km resolution grid. For example, Fig. 3b shows an example of MODIS Terra LST on 5 August 2004 around the Baltoro glacier, a time slice that was selected for the low number of missing values in this region. MODIS exceeds the melting point over most of the glacier, including over smaller, largely debris-free

TCD
9, 2259–2299, 2015

tributary glaciers, due to blending with valley rock walls. The data are also warmer over glacier areas with debris-covered fractions that fall below the threshold of 40 % used to define a WRF pixel as a debris-covered (cf. Fig. 2b). Therefore, the binary definition of debris-free and debris-covered glacier surface types, as well as inaccuracies in the glacier mask, likely contribute to colder LST in WRF-CMB.

To examine temporal variations, Fig. 3c shows a time series of daytime and nightime LST for July and August 2004 from all three datasets at a pixel on the Baltoro glacier tongue, which is denoted by a black circle on Fig. 3b. This pixel was selected since it falls within the glacier outline on the MODIS grid and because the debris coverage in 2004 appears to be ~ 100 % (cf. Fig. 2 in Mihalcea et al., 2008). The variability in LST at this point is well captured in DEB, including days with maxima exceeding ~ 30 °C and warmer or cooler periods, while as expected CLN greatly underpredicts LST and its variability.

3.2 Glacier surface-energy and climatic-mass dynamics

The basin-mean cumulative glacier CMB for both simulations is shown in Fig. 4a. The month of May is characterized by basin-mean accumulation (Fig. 4b), consistent with the findings of Maussion et al. (2014) of the importance of spring precipitation in this region. On average, the melt season lasts from approximately mid-June until mid-to-end of September, over which period ~ 55 % of grid cells categorized as debris-covered are exposed. As a result, there is a significant decrease in net ablation, as is discussed at the end of this section. Note that the basin-averaged MB during summer is significantly less negative than in a previous clean-ice model run (Collier et al., 2013), which is primarily due to increased precipitation as a result of changing the atmospheric diffusion scheme (Table 1) through the albedo effect. The decrease in ablation is likely an improvement, since the previous estimate showed a negative bias in comparison with in situ glaciological measurements. To isolate the impacts of debris, we focus on the period of 1 July to 1 October 2004 for the remainder of the analysis, when more than 15 % of debris pixels are exposed on average over the Karakoram.

TCD
9, 2259–2299, 2015

The mean vertical balance profile indicates the equilibrium line altitude (ELA) between 1 July and 1 October 2004 is located at ~ 5250 m a.s.l. (Fig. 5), which is higher than previous estimates of annual ELAs in the Karakoram of 4200 to 4800 m (Young and Hewitt, 1993), due to focus on the ablation season and the absence of avalanche accumulation. The latter factor is important in this region and produces ELAs that are often located hundreds of meters below the climatic snowline (e.g. Benn and Lehmkuhl, 2000; Hewitt, 2005, 2011). Below the simulated ELA, there is a ~ 10 % reduction in total ablation in DEB compared with CLN (2.1 m w.e.), which we anticipate represents an underestimate due to the non-linear debris thickness observed near the Baltoro terminus. To further elucidate the impact of debris, we focus on elevational profiles in our analysis, since above the mean elevation of the snow line at ~ 4500 m a.s.l., surface-energy fluxes in the two simulations are indistinguishable (and note that the discrepancy between the snow line and ELA results from strong accumulation prior to 1 July).

The presence of debris cover has only a small impact on basin-mean surface-energy fluxes between 1 July and 1 October 2004 (Table 4). However, elevational profiles of reveal a strong influence of debris in the ablation areas (Fig. 6b). Net shortwave radiation (SWnet) increases due to the lower surface albedo, while net longwave radiation (LWnet) becomes more negative due to stronger emission by warmer debris surfaces. The turbulent flux of sensible heat becomes a smaller energy source or even sink, while that of latent heat (QL) becomes slightly more negative. The conductive heat flux (QC) transitions from a small energy gain in CLN to a strong sink in DEB due to solar heating of the debris, and extracts nearly twice as much energy from the surface as LWnet at the lowest glaciated elevations. Penetrating shortwave radiation (QPS) becomes negligible in DEB as the overlying snow cover goes to zero, while in CLN this flux becomes a stronger energy sink, due to the lower extinction coefficient of ice (Bintanja and van den Broeke, 1995). These changes in the surface-energy dynamics produce only a small decrease in total snow and ice melt in the ablation zones (Table 4; Fig. 6c), with the near zero difference above 4000 m reflecting overlying snow cover

TCD
9, 2259–2299, 2015

and some compensating increases in melt under thinner debris, which are prevalent (cf. Fig. 2c). Surface vapour fluxes are small when spatially and temporally averaged; however, they represent a non-negligible mass flux in total, with $\sim 1.3 \times 10^5$ kg of sublimation and 3.2×10^4 kg of deposition at snow and ice surfaces. Vapour exchange between the debris and the atmosphere also totals -1.2×10^4 kg over the simulation period, although net changes in debris moisture storage are approximately zero.

Simulated daily mean ablation (corresponding to sub-debris-ice and total-column values in DEB and CLN, respectively) shows a general decrease with both topographic height and debris thickness increase (Fig. 7). Although melt rates below 3500 m have been estimated to be small, as a result of insulation by thick debris cover (Hewitt, 2005), our results suggest that appreciable rates, of up to ~ 2 cm w.e. day^{-1} occur under the thickest layers at lower elevations. For the thinnest debris layers (of a few centimeters), ablation is enhanced in DEB compared with CLN. Simulated values are consistent with the few available field measurements of glacier ablation in this region. For example, Mayer et al. (2010) reported rates of ~ 2 to 14 cm w.e. day^{-1} under debris covers of ~ 1 to 38 cm on the Hinarche glacier (74° 43′ E, 36° 5′ N) in 2008. Mihalcea et al. (2006) reported rates of 1–6 cm w.e. d^{-1} on the Baltoro glacier in 2004 over elevations of $\sim$ 4000–4700 m and thicknesses of 0 to 18 cm, and the modelled melt rates over a similar period compare well with their Østrem curve (cf. their Fig. 7).

A spatial plot of the total accumulated mass balance in DEB delineates regions of glacier mass gain and loss (Fig. 8a) in the Karakoram. Accumulation is higher in the western part of the domain, where more precipitation falls over the simulation period (not shown). Differences between DEB and CLN are small over most of the basin, with the exception of lower altitude glacier tongues where differences reach 2.5 m w.e. (Fig. 8b). The strong decrease in mass loss in these areas increases the basin-mean final mass balance from -327.4 kg m^{-2} in CLN to -305.0 in DEB.

TCD
9, 2259–2299, 2015

3.3 Atmosphere-glacier feedbacks

The total number of hours for which the surface temperature reaches or exceeds the melting point (here denoted as "melt hours") ranges from more than 1500 at low-altitude glacier termini to less than 50 above ~ 6000 m (Fig. 9a). The presence of debris results in upwards of 800 additional melt hours in DEB compared with CLN (Fig. 9b). These additional melt hours provide a strong heat flux to the atmosphere, with an extra 2.5×10^7 W of energy transferred to the atmosphere in DEB by the sensible heat flux.

The change in surface boundary conditions produces higher basin-mean near-surface air temperatures, of up to 2–3 K at the lowest glaciated elevations (Fig. 10a), consistent with observations of higher air temperatures over debris-covered glacier areas during the ablation season (Takeuchi et al., 2000, 2001; Reid et al., 2012). Basin-mean accumulated precipitation is similar between the two simulations and ranges from 50–150 mm below 5000 m and increases approximately linearly with elevation above this level. The simulated frozen fraction increases approximately linearly from 10 % at 3000 m to more than 90 % at and above ~ 5250 m (not shown). These results are consistent with estimates of annual precipitation, which indicate that valleys are drier and precipitation increases up towards accumulation areas, and with previously reported frozen fractions (Winiger et al., 2005; Hewitt, 2005). Finally, higher surface roughness values over debris result in a small decrease of near-surface horizontal wind speeds (Fig. 10c). Mean elevational gradients in near-surface meteorological fields are provided in Table 5 where the variation is approximately linear. It is noteworthy that changes in atmosphere-glacier feedbacks due to the presence of surficial debris also help to drive the differences in observed ablation (cf. Figs. 6 and 7).

The atmospheric surface layer becomes less stable on average due to solar heating of exposed debris (not shown), which enhances turbulent mixing and convective overturning. As a result, the elevational gradient in the mean planetary boundary layer (PBL) height is reversed in DEB below 4500 m, with a mixed layer depth of approximately four times that in CLN at 3000 m (Fig. 11a). Focussing on exposed debris pixels

TCD
9, 2259–2299, 2015

only, peak PBL depths reach 1.5 km during the day in DEB compared with only a couple hundred meters in CLN (Fig. 11b). The development of a convective mixed layer also starts approximately two hours earlier on average, shortly after 7 a.m. LT.

4 Discussion and conclusions

In this study, surficial debris was introduced to the coupled atmosphere-glacier modelling system, WRF-CMB. The model provides a unique tool for investigating the influence of debris cover on both Karakoram glaciers and atmosphere-glacier interactions in an explicitly resolved framework. The impact of debris was examined for the period of 1 May to 1 October 2004. The findings presented in this study have important implications for glacio-hydrological studies in the Karakoram, as they confirm that neglecting supraglacial debris will result in an overestimation of glacier mass loss during the ablation season, of ∼ 7 % over the whole basin and exceeding 2.5 m w.e. at the lowest elevations. In addition, exposed debris alters near-surface meteorological fields and their elevational gradients, which are often key modelling parameters used to extrapolate forcing data from a point location (e.g., an automatic weather station) over the rest of the glacier surface (e.g. Marshall et al., 2007; Gardner et al., 2009; Reid et al., 2012). For temperature, the lapse rate at lower elevations is more than 1° steeper in DEB, as a result of surface temperatures exceeding the melting point and a higher net turbulent transfer of sensible heat to the atmosphere that produces higher near-surface air temperatures. The simulated lapse rate is steeper than values reported for debris-covered glaciers spanning a smaller elevational extent (Reid et al., 2012) and in high-altitude catchments in the eastern Himalaya, where the monsoon circulation system plays a more pronounced role (Immerzeel et al., 2014b). Finally, accounting for vapour fluxes from the debris increases the net loss by 3.7 % compared with CLN and comprises 8.7 % of the total negative mass flux in DEB, with implications for neglecting QL in a surface energy balance calculation, as is frequently done in numerical studies of debris cover.

TCD
9, 2259–2299, 2015

Simulated ice-ablation rates in DEB under thicker debris covers at lower elevations are consistent with the findings of Mihalcea et al. (2006) of non-negligible melt energy under debris covers exceeding 1 m using a degree-day modelling approach on the Baltoro glacier, and with the measured rates reported by Mayer et al. (2010). The authors of the latter study suggest the mechanism is more efficient heat transfer in the debris in the presence of moisture during the ablation season despite its thickness. In this study, mean ice-melt rates for pixels with debris thickness exceeding 20 cm show only some correlation with the debris moisture content ($R^2 = 0.39$). Near-surface air temperature ($R^2 = 0.90$) is likely a stronger driver of the simulated melt rates below thick debris. The interactive nature of the simulation may also permit a positive feedback mechanism, in which higher surface temperatures over thicker debris transfer energy to the atmosphere, which in turn promotes higher air temperature and further melt. In combination with surface heteorogeneity in the ablation zone (e.g., the presence of meltwater ponds and ice cliffs) and recent changes in ice flow velocities (Quincey et al., 2009; Scherler and Strecker, 2012), both the simulated melt rates under thicker debris and enhanced melt under thinner debris help to explain the lack of significant differences in recent elevation changes between debris-free and debris-covered glacier surfaces in the Karakoram (Gardelle et al., 2013).

The alterations to the glacier energy and mass fluxes and to atmosphere-glacier interactions presented in this study likely represent an underestimate, since approximately 45 % of debris-covered pixels remained snow-covered and also due to potential non-linear effects near glacier termini. The relatively small percentage of exposed pixels may result from interannual variability in accumulation, since the clean snow/ice mask of Kääb et al. (2012) used to delineate debris-covered areas was generated from Landsat data from the year 2000, and to our binary assignment of surface types as "debris-covered" or "debris-free", in which the 40 % threshold would tend to increase the altitude of the debris-covered area. Finally, overestimation of nighttime cooling resulting from excessive damping of QS in stable conditions could also contribute to an

TCD
9, 2259–2299, 2015

underestimation of snowmelt, which points to the need to improve the stability corrections for interactive applications at high altitudes.

The exact glaciological and meteorological changes are sensitive (i) to the fact that we have only simulated the ablation season of 2004 and (ii) to the debris thickness specification itself, which is specified simply in this study. There have been numerous recent efforts to more precisely determine debris thickness fields using satellite-derived surface temperature fields (e.g. Suzuki et al., 2007; Mihalcea et al., 2008; Foster et al., 2012; Brenning et al., 2012), which is an appealing solution due to the wide spatial and temporal coverage of remote sensing data. However, none of these studies have successfully reproduced field measurements without using empirically-determined relationships or calibration factors (Mihalcea et al., 2008; Foster et al., 2012). These methods are therefore best suited for debris-covered glaciers for which the necessary measurements to compute the relationships or factors are available, and their applicability for regional-scale studies such as this one is uncertain. Evaluating the impact of using a more accurate and detailed debris thickness field for the Karakoram, as well as accounting for sub-grid scale heterogeneity (for example, by introducing a treatment of ice cliffs; Reid and Brock, 2014), remain important future steps for more spatially detailed studies of glacier CMB in this region. Nonetheless, by providing an estimate of the controlling influence of debris, these simulations contribute to a greater understanding of glacier behaviour in the Karakoram.

Acknowledgements. The authors thank G. Diolaiuti for providing the debris thickness data of Mihalcea et al. (2008), whose field and laboratory work was completed as a part of the SHARE (Station at High Altitude for Research on the Environment) project and supported by EvK2CNR. E. Collier was supported by a Queen Elizabeth II graduate scholarship. L. Nicholson is funded by an Austrian Science Fund (FWF Grant V309). F. Maussion acknowledges support by the Austrian Science Fund (FWF project P22443-N21). A.B.G. Bush acknowledges support from the Natural Sciences and Engineering Research Council, and the Canadian Institute for Advanced Research (Earth System Evolution Program). The supercomputing resources for this study were provided by Compute/Calcul Canada (https://computecanada.ca) and WestGrid (https://www.westgrid.ca). This work was partly carried out under the Collaborative Adapta-

TCD
9, 2259–2299, 2015

tion Research Initiative in Africa and Asia (CARIAA) with financial support from the UK Government's Department for International Development and the International Development Research Centre, Ottawa, Canada. The views expressed in this work are those of the creators and do not necessarily represent those of the UK Government's Department for International Development, the International Development Research Centre, Canada or its Board of Governors.

References

Benn, D. I. and Lehmkuhl, F.: Mass balance and equilibrium-line altitudes of glaciers in high-mountain environments, Quatern. Int., 65, 15–29, 2000. 2271

Bintanja, R. and van den Broeke, M. R.: The surface energy balance of Antarctic snow and blue ice, J. Appl. Meteorol., 34, 902–926, 1995. 2271

Bolch, T., Kulkarni, A., Kääb, A., Huggel, C., Paul, F., Cogley, J. G., Frey, H., Kargel, J. S., Fujita, K., Scheel, M., Bajracharya, S., and Stoffel, M.: The state and fate of Himalayan glaciers, Science, 336, 310–314, 2012. 2261

Braithwaite, R. J.: Aerodynamic stability and turbulent sensible-heat flux over a melting ice surface, the Greenland ice sheet, J. Glaciol., 41, 562–571, 1995. 2266

Brenning, A., Peña, M. A., Long, S., and Soliman, A.: Thermal remote sensing of ice-debris landforms using ASTER: an example from the Chilean Andes, The Cryosphere, 6, 367–382, doi:10.5194/tc-6-367-2012, 2012. 2276

Brock, B. W., Mihalcea, C., Kirkbride, M. P., Diolaiuti, G., Cutler, M. E., and Smiraglia, C.: Meteorology and surface energy fluxes in the 2005–2007 ablation seasons at the Miage debris-covered glacier, Mont Blanc Massif, Italian Alps, J. Geophys. Res., 115, D09106, doi:10.1029/2009JD013224, 2010. 2262, 2267, 2286

Brodzik, M. J., Armstrong, R., and Savoie, M.: Global EASE-Grid 8-day Blended SSM/I and MODIS Snow Cover, National Snow and Ice Data Center, Boulder, Colorado, USA, Digital media, 2007. 2264

Chen, F. and Dudhia, J.: Coupling an advanced land surface-hydrology model with the Penn State – NCAR MM5 modelling system. Part I: Model implementation and sensitivity, Mon. Weather Rev., 129, 569–585, 2001. 2263

TCD
9, 2259–2299, 2015

Clark Jr., S. P. (Ed.): Thermal conductivity, in: Handbook of Physical Constants – Revised Edition, The Geological Society of America Memoir 97, Geological Society of America, New York, 459–482, 1966. 2265, 2286

Cogley, J. G.: Present and future states of Himalaya and Karakoram glaciers, Ann. Glaciol., 52, 69–73, 2011. 2261

Collier, E., Mölg, T., Maussion, F., Scherer, D., Mayer, C., and Bush, A. B. G.: High-resolution interactive modelling of the mountain glacier–atmosphere interface: an application over the Karakoram, The Cryosphere, 7, 779–795, doi:10.5194/tc-7-779-2013, 2013. 2262, 2263, 2264, 2265, 2270, 2286

Collier, E., Nicholson, L. I., Brock, B. W., Maussion, F., Essery, R., and Bush, A. B. G.: Representing moisture fluxes and phase changes in glacier debris cover using a reservoir approach, The Cryosphere, 8, 1429–1444, doi:10.5194/tc-8-1429-2014, 2014. 2265

Collins, W. D., Rasch, P. J., Boville, B. A., Hack, J. J., McCaa, J. R., Williamson, D., L., Kiehl, J., T., Briegleb, B., Bitz, C., Lin, S- J., Zhang, M., and Dai, Y.: Description of the NCAR Community Atmosphere Model (CAM3.0). Technical Note TN-464+STR, National Center for Atmos. Res. Atmospheric Research, Boulder, CO, 214 pp., 2004. 2284

Conway, H. and Rasmussen, L. A.: Summer temperature profiles within supraglacial debris on Khumbu Glacier, Nepal, IAHS-AISH P., 264, 89–97, 2000. 2265, 2286

Conway, J. P. and Cullen, N. J.: Constraining turbulent heat flux parameterization over a temperate maritime glacier in New Zealand, Ann. Glaciol., 54, 41–51, 2013. 2266

Copland, L., Sylvestre, T., Bishop, M. P., Shroder, J. F., Seong, Y. B., Owen, L. A., Bush, A.B.G, and Kamp, U.: Expanded and recently increased glacier surging in the Karakoram, Arct. Antarct. Alp. Res., 43, 503–516, 2011.

Daly, R. A., Manger, G. E., Clark Jr., S. P.: Density of Rocks. In: Handbook of Physical Constants – Revised Edition, The Geological Society of America Memoir 97, edited by: Clark Jr., S. P., New York, Geological Society of America, 19–26, 1966. 2265, 2286

Dee, D. P., Uppala, S. M., Simmons, A. J., Berrisford, P., Poli, P., Kobayashi, S., Andrae, U., Balmaseda, M. A., Balsamo, G., Bauer, P., Bechtold, P., Beljaars, A. C. M., van de Berg, L., Bidlot, J., Bormann, N., Delsol, C., Dragani, R., Fuentes, M., Geer, A. J., Haimberger, L., Healy, S. B., Hersbach, H., Hlm, E. V., Isaksen, L., Kållberg, P., Köhler, M., Matricardi, M., McNally, A. P., Monge-Sanz, B. M., Morcrette, J.-J., Park, B.-K., Peubey, C., de Rosnay, P., Tavolato, C., Thpaut, J.-N., and Vitart, F.: The ERA-Interim reanalysis: configuration and

TCD
9, 2259–2299, 2015

performance of the data assimilation system, Q. J. Roy. Meteor. Soc., 137, 553–597, 2011. 2264, 2284
Foster, L. A., Brock, B. W., Cutler, M. E. J., and Diotri, F.: A physically based method for estimating supraglacial debris thickness from thermal band remote-sensing data, J. Glaciol., 58, 677–691, 2012. 2276
Fujii, Y.: Experiment on glacier ablation under a layer of debris cover, J. Japan. Soc. Snow Ice (Seppyo), 39, 20–21, 1977. 2261
Gardelle, J., Berthier, E., and Arnaud, Y.: Slight mass gain of Karakoram glaciers in the early twenty-first century, Nat. Geosci., 5, 322–325, 2012. 2261
Gardelle, J., Berthier, E., Arnaud, Y., and Kääb, A.: Region-wide glacier mass balances over the Pamir-Karakoram-Himalaya during 1999–2011, The Cryosphere, 7, 1263–1286, doi:10.5194/tc-7-1263-2013, 2013. 2261, 2275
Gardner, A. S., Sharp, M. J., Koerner, R. M., Labine, C., Boon, S., Marshal, S. J., Burgess, D. O., and Lewis, E.: Near-surface temperature lapse rates over Arctic glaciers and their implications for temperature downscaling, J. Climate, 22, 4281–4298, 2009. 2274
Giesen, R. H., Andreassen, L. M., van den Broeke, M. R., and Oerlemans, J.: Comparison of the meteorology and surface energy balance at Storbreen and Midtdalsbreen, two glaciers in southern Norway, The Cryosphere, 3, 57–74, doi:10.5194/tc-3-57-2009, 2009. 2266
Granger, R. J., Pomeroy, J. W., and Parviainen, J.: Boundary layer integration approach to advection of sensible heat to a patchy snow cover, 59th Eastern Snow Conference, Vermont, USA, 147–159, 5–7 June 2002. 2262
Hewitt, K.: The Karakoram anomaly? Glacier expansion and the "elevation effect" Karakoram Himalaya, Mt. Res. Dev., 25, 332–340, 2005. 2261, 2271, 2272, 2273
Hewitt, K.: Glacier change, concentration, and elevation effects in the Karakoram Himalaya, Upper Indus Basin, Mt. Res. Dev., 31, 188–200, 2011. 2261, 2271
Hong, S.-Y., Noh, Y., and Dudhia, J.: A new vertical diffusion package with an explicit treatment of entrainment processes, Mon. Weather Rev., 134, 2318–2341, 2006. 2284
Immerzeel, W. W., Kraaijenbrink, P. D. a., Shea, J. M., Shrestha, A. B., Pellicciotti, F., Bierkens, M. F. P., and de Jong, S. M.: High-resolution monitoring of Himalayan glacier dynamics using unmanned aerial vehicles, Remote Sens. Environ., 150, 93–103, 2014a. 2269
Immerzeel, W. W., Petersen, L., Ragettli, S., and Pellicciotti, F.: The importance of observed gradients of air temperature and precipitation for modeling runoff from a glacierized watershed in

TCD
9, 2259–2299, 2015

the Nepalese Himalaya, Water Resour. Res., 50, 2212–2226, doi:10.1002/2013WR014506, 2014b. 2274
Inoue, J. and Yoshida, M.: Ablation and heat exchange over the Khumbu Glacier, J. Japan. Soc. Snow Ice (Seppyo), 39, 7–14, 1980. 2261, 2262, 2269
Jiménez, P. A., Dudhia, J., González-Rouco, J. F., Navarro, J., Montávez, J. P., and García-Bustamante, E.: A revised scheme for the WRF surface layer formulation, Mon. Weather Rev., 140, 898–918, 2012. 2284
Kain, J. S.: The Kain–Fritsch convective parameterization: An update, J. Appl. Meteorol., 43, 170–181, 2004. 2284
Kääb, A., Berthier, E., Nuth, C., Gardelle, J., and Arnaud, Y.: Contrasting patterns of early twenty-first-century glacier mass change in the Himalayas, Nature, 488, 495–498, 2012. 2261, 2267, 2275
Kaser, G., Großhauser, M., and Marzeion, B.: Contribution potential of glaciers to water availability in different climate regimes, P. Natl. Acad. Sci. USA, 107, 20223–20227, 2010. 2261
Loomis, S. R.: Morphology and ablation processes on glacier ice, Assoc. Am. Geogr. Proc., 2, 88–92, 1970. 2268
Lutz, A. F., Immerzeel, W. W., Shrestha, A. B., and Bierkens, M. F. P.: Consistent increase in High Asia's runoff due to increasing glacier melt and precipitation, Nat. Clim. Chang., 4, 1–6, 2014. 2261
Marshall, S. J., Sharp, M. J., Burgess, D. O., and Anslow, F. S.: Surface temperature lapse rate variability on the Prince of Wales Ice-eld, Ellesmere Island, Canada: implications for regional-scale downscaling of temperature, Int. J. Climatol., 27, 385–398, 2007. 2274
Martin, E. and Lejeune, Y.: Turbulent fluxes above the snow surface, Ann. Glaciol., 26, 179–183, 1998. 2266
Mattson, L. E., Gardner, J. S., and Young, G. J.: Ablation on debris covered glaciers: an example from the Rakhiot Glacier, Punjab, Himalaya, Snow and Glacier Hydrology, IAHS-AISH P., 218, 289–296, 1993. 2268
Maussion, F., Scherer, D., Mölg, T., Collier, E., Curio, J., and Finkelnburg, R.: Precipitation seasonality and variability over the Tibetan Plateau as resolved by the High Asia Reanalysis, J. Climate, 27, 1910–1927, 2014. 2270
Mayer, C., Lambrecht, A., Mihalcea, C., Belo, M., Diolaiuti, G., Smiraglia, C., and Bashir, F.: Analysis of glacial meltwater in Bagrot Valley, Karakoram, Mt. Res. Dev., 30, 169–177, 2010. 2272, 2275

TCD
9, 2259–2299, 2015

Mayer, C., Lambrecht, A., Oerter, H., Schwikowski, M., Vuillermoz, E., Frank, N., and Diolaiuti, G.: Accumulation studies at a high elevation glacier site in Central Karakoram, Adv. Meteorol., 2014, 1–12, 2014. 2261

Mihalcea, C., Mayer, C., Diolaiuti, G., Smiraglia, C., and Tartari, G.: Ablation conditions on the debris covered part of Baltoro Glacier, Karakoram, Ann. Glaciol., 43, 292–300, 2006. 2261, 2267, 2272, 2275

Mihalcea, C., Mayer, C., Diolaiuti, G., D'Agata, C., Smiraglia, C., Lambrecht, A., Vuillermoz, E., and Tartari, G.: Spatial distribution of debris thickness and melting from remote-sensing and meteorological data, at debris-covered Baltoro glacier, Karakoram, Pakistan, Ann. Glaciol., 48, 49–57, 2008. 2261, 2267, 2268, 2270, 2276

Molinari, J. and Dudek, M.: Parameterization of convective precipitation in mesoscale numerical-models – a critical-review, Mon. Weather Rev., 120, 326–344, 1992. 2264

Mölg, T., Cullen, N. J., Hardy, D. R., Kaser, G., and Klok, E. J.: Mass balance of a slope glacier on Kilimanjaro and its sensitivity to climate, Int. J. Climatol., 28, 881–892, 2008. 2264, 2266

Mölg, T., Cullen, N. J., Hardy, D. R., Winkler, M., and Kaser, G.: Quantifying climate change in the tropical midtroposphere over East Africa from glacier shrinkage on Kilimanjaro, J. Climate, 22, 4162–4181, 2009. 2264, 2266

Nicholson, L. and Benn, D.: Properties of natural supraglacial debris in relation to modelling sub-debris ice ablation, EPSL, 38, 490–501, 2012. 2262, 2265, 2267, 2286

Niu, G.-Y., Yang, Z.-L., Mitchell, K. E., Chen, F., Ek, M. B., Barlage, M., Kumar, A., Manning, K., Niyogi, D., Rosero, E., Tewari, M., and Youlong, X.: The community Noah land surface model with multiparameterization options (Noah-MP): 1. Model description and evaluation with local-scale measurements, J. Geophys. Res., 116, D12109, doi:10.1029/2010JD015139, 2011. 2263, 2266, 2284

Østrem, G.: Ice melting under a thin layer of moraine, and the existence of ice cores in moraine ridges, Geogr. Ann., 41, 228–230, 1959. 2261, 2268

Pellicciotti, F., Stephan, C., Miles, E., Immerzeel, W. W., and Bolch, T.: Mass balance changes of the debris-covered glaciers in the Langtang Himal in Nepal between 1974 and 1999, J. Geophys. Res., in press, 1–27, 2015. 2269

Pfeffer, W. T., Arendt, A., Bliss, A., Bolch, T., Cogley, J. G., Gardner, A. S., Hagen, J.-O., Hock, R., Kaser, G., Kienholz, C., Miles, E. S., Moholdt, G., Mölg, N., Paul, F., Radic, V., Rastner, P., Raup, B. H., Rich, J., and Sharp, M. J.: The Randolph Glacier Inventory: a globally complete inventory of glaciers, J. Glaciol., 221, 537–552, 2014. 2264

TCD
9, 2259–2299, 2015

Quincey, D. J., Copland, L., Mayer, C., Bishop, M., Luckman, A., and Belo, M.: Ice velocity and climate variations for Baltoro Glacier, Pakistan, J. Glaciol., 55, 1061–1071, 2009. 2275
Rankl, M., Kienholz, C., and Braun, M.: Glacier changes in the Karakoram region mapped by multimission satellite imagery, The Cryosphere, 8, 977–989, doi:10.5194/tc-8-977-2014, 2014. 2264, 2267, 2268, 2290
Reid, T. D. and Brock, B. W.: An energy-balance model for debris-covered glaciers including heat conduction through the debris layer, J. Glaciol., 56, 903–916, 2010. 2286
Reid, T. D. and Brock, B. W.: Assessing ice-cliff backwasting and its contribution to total ablation of debris-covered Miage glacier, Mont Blanc massif, Italy, J. Glaciol., 60, 3–13, 2014. 2276
Reid, T. D., Carenzo, M., Pellicciotti, F., and Brock, B. W.: Including debris cover effects in a distributed model of glacier ablation, J. Geophys. Res., 117, D18105, doi:10.1029/2012JD017795, 2012. 2262, 2266, 2267, 2273, 2274
Sakai, A., Nakawo, M., and Fujita, K.: Melt rate of ice cliffs on the Lirung Glacier, Nepal Himalayas, 1996, Bull. Glacier Res., 16, 57–66, 1998. 2269
Sakai, A., Takeuchi, N., Fujita, K., and Nakawo, N.: Role of supraglacial ponds in the ablation process of a debris-covered glacier in the Nepal Himalaya. Debris-Covered Glaciers, IAHS-AISH P., 264, 119–130, 2000. 2269
Scherler, D. and Strecker, M. R.: Large surface velocity fluctuations of Biafo Glacier, central Karakoram, at high spatial and temporal resolution from optical satellite images, J. Glaciol., 58, 569–580, 2012. 2275
Scherler, D., Bookhagen, B., and Strecker, M. R.: Spatially variable response of Himalayan glaciers to climate change affected by debris cover, Nat. Geosci., 4, 156–159, 2011. 2261
Skamarock, W. C. and Klemp, J. B.: A time-split nonhydrostatic atmospheric model for weather research and forecasting applications, J. Comput. Phys., 227, 3465–3485, 2008. 2263
Suzuki, R., Fujita, K., and Ageta, Y.: Spatial distribution of thermal properties on debris-covered glaciers in the Himalayas derived from ASTER data, Bull. Glaciol. Res., 24, 13–22, 2007. 2276
Takeuchi, Y., Kayastha, R. B., and Nakawo, M.: Characteristics of ablation and heat balance in debris-free and debris-covered areas on Khumbu glacier, Nepal Himalayas, in the premonsoon season, in: Debris-covered glaciers, IAHS-AISH P., 264, 53–61, 2000. 2273
Takeuchi, Y., Kayastha, R. B., Naito, N., Kadota, T., and Izumi, K.: Comparison of meteorological features in the debris-free and debris-covered areas at Khumbu Glacier, Nepal Himalayas, in the premonsoon season, 1999, Bull. Glaciol. Res., 18, 15–18, 2001. 2262, 2273

TCD
9, 2259–2299, 2015

Thompson, G., Field, P. R., Rasmussen, R. M., and Hall, W. D.: Explicit forecasts of winter precipitation using an improved bulk microphysics scheme. Part II: Implementation of a new snow parameterization, Mon. Weather Rev., 136, 5095–5115, 2008. 2284

Weisman, M. L., Skamarock, W. C., and Klemp, J. B.: The resolution dependence of explicitly modeled convective systems, Mon. Weather Rev., 125, 527–548, 1997. 2264

Winiger, M., Gumpert, M., and Yamout, H.: Karakorum–Hindukush–western Himalaya: assessing high-altitude water resources, Hydrol. Process., 19, 2329–2338, 2005. 2273

Young, G. J. and Hewitt, K.: Glaciohydrological features of the Karakoram Himalaya: measurement possibilities and constraints, in: Proceedings of the Kathmandu Symposium – Snow and Glacier Hydrology, IAHS-AISH P., 218, 273–283, 1993. 2271

Zhang, Y., Fujita, K., Liu, S., Liu, Q., and Nuimura, T.: Distribution of debris thickness and its effect on ice melt at Hailuogou glacier, southeastern Tibetan Plateau, using in situ surveys and ASTER imagery, J. Glaciol., 57, 1147–1157, 2011. 2267

TCD
9, 2259–2299, 2015

Table 1. WRF configuration.

Model configuration		
Horizontal grid spacing	30, 10, 2 km (domains 1–3)	
Vertical levels	40	
Model top pressure	50 hPa	
Model physics		
Radiation	CAM	Collins et al. (2004)
Microphysics	Thompson	Thompson et al. (2008)
Cumulus	Kain–Fritsch (none in D3)	Kain (2004)
Atmospheric boundary layer	Yonsei University	Hong et al. (2006)
Surface layer	Monin–Obukhov (revised MM5)	Jiménez et al. (2012)
Land surface	Noah–MP	Niu et al. (2011)
Dynamics		
Top boundary condition	Rayleigh damping	
Horizontal diffusion	Computed in physical space	
Lateral boundaries		
Forcing	ERA Interim, T255 spectral resolution updated 6 hourly	Dee et al. (2011)

TCD
9, 2259–2299, 2015

Table 2. Subsurface layer depths.

Snow	variable
Debris	every 0.01 m
Ice	0.1, 0.2, 0.3, 0.4, 0.5, 1.0, 1.5, 2.0, 2.5, 3.0, 3.5, 4.0, 5.0, 7.0 m

TCD
9, 2259–2299, 2015

Table 3. Physical properties in the CMB model.

Density ($kg\,m^{-3}$)		
ice	915	–
whole rock	2700	Daly et al. (1966)
water	1000	–
Specific heat capacity ($J\,kg^{-1}\,K^{-1}$)		
air	1005	–
ice	2106	–
whole rock	750	Clark (1966)
water	4181	–
Thermal conductivity ($W\,m^{-1}\,K^{-1}$)		
air	0.024	–
ice	2.51	–
whole rock	2.50	Conway and Rasmussen (2000)
water	0.58	–
Surface roughness length (m^{-1})		
ice	0.001	Reid and Brock (2010)
debris	0.016	Brock et al. (2010)
Albedo		
ice	0.30	Collier et al. (2013)
firn	0.55	Collier et al. (2013)
fresh snow	0.85	Collier et al. (2013)
debris	0.20	Nicholson and Benn (2012)
Emissivity		
ice/snow	0.97	Reid and Brock (2010)
debris	0.94	Brock et al. (2010)

TCD
9, 2259–2299, 2015

Table 4. Mean glacier surface-energy and climatic-mass fluxes.

Surface energy fluxes ($W m^{-2}$)	DEB	CLN
net shortwave (SWnet)	93.2	88.9
net longwave (LWnet)	−77.5	−76.0
sensible heat (QS)	10.0	12.1
latent heat (QL)	−7.4	−7.1
conduction (QC)	3.8	13.8
penetrating SW (QPS)	−4.8	−7.7
precipitation (QPRC)	~ 0	~ 0
Mass fluxes ($kg m^{-2}$)	**DEB**	**CLN**
surface melt	−0.18	−0.26
subsurface melt	−0.09	−0.03
snow refreeze	0.08	0.08
sublimation	−0.01	−0.01
deposition	~ 0	~ 0
evaporation	~ 0	–
condensation	~ 0	–
surface accumulation	0.03	0.03

TCD
9, 2259–2299, 2015

Table 5. Elevational gradients.

	Below 5000 m DEB	CLN	5000–7000 m DEB
2 m air temperature [$K\,m^{-1}$]	−0.0074	−0.0062	−0.0074
10 m wind speed [$m\,s^{-1}\,m^{-1}$]	0.0009	0.0007	0.002
Accum. precipitation [$mm\,m^{-1}$]	–	–	0.066

TCD
9, 2259–2299, 2015

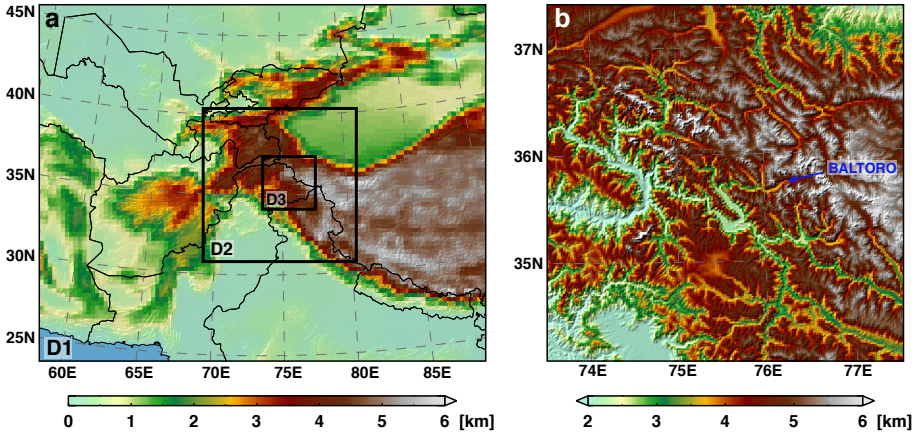

Figure 1. Topographic height shaded in units of km for **(a)** all three model domains in WRF-CMB, which are centered over the Karakoram and configured with grid spacings of 30, 10 and 2 km, and **(b)** a zoom-in of the finest resolution domain, WRF D3.

TCD
9, 2259–2299, 2015

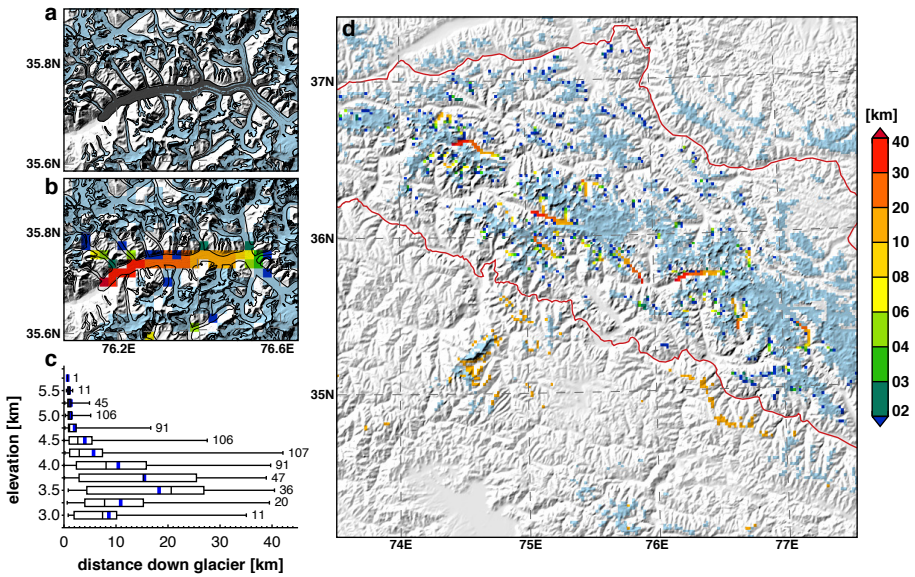

Figure 2. (a) debris-covered (grey) and debris-free (blue) glacier areas, calculated on a high-resolution (40 m) grid for the Baltoro glacier and surrounding areas. The distance down-glacier over debris-covered areas, which is multipled by a fixed gradient to map debris, is shown for **(b)** the Baltoro glacier and **(d)** the entire WRF-D3 region. In **(d)**, the red line delineates the region where centerline information was available from (Rankl et al., 2014). **(c)** A box plot of debris thicknesses values for 250 m elevation bins in WRF D3. The thick-blue and thin-black lines indicate the mean and median thicknesses in each bin and the total number of debris-covered pixels is given as a text string at the upper end of the range.

TCD
9, 2259–2299, 2015

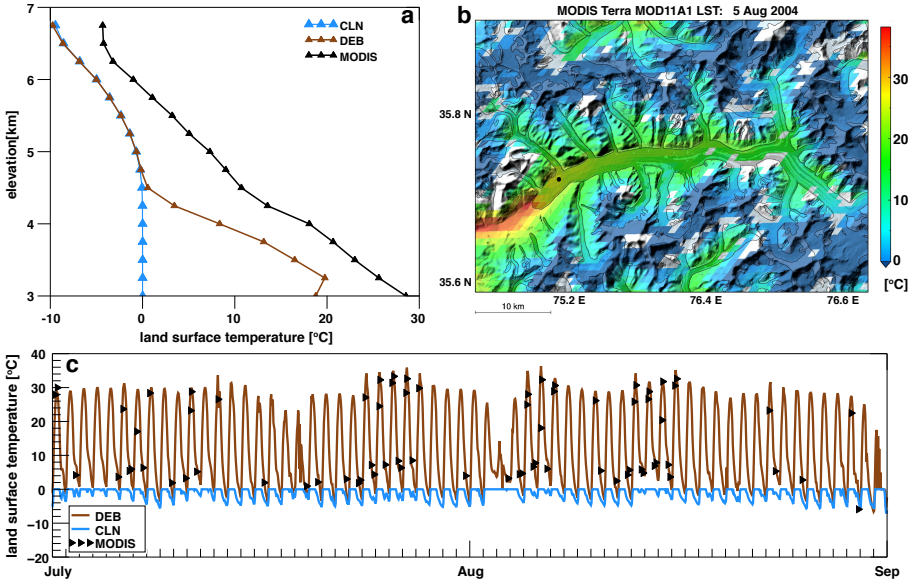

Figure 3. (a) Mean elevational profiles of daytime land surface temperature from DEB, CLN, and composite MODIS Terra MOD11A1/Aqua MYD11A1 datasets, averaged from 1 June to 1 September 2004 and in 250 m elevation bins over glaciated pixels in WRF. **(b)** A sample time slice of MODIS Terra LST from 5 August 2004 on its native grid, overlaid on the Baltoro glacier outline and debris-covered area. **(c)** Time series of LST from 1 July to 1 September 2004 from the same datasets as in panel **(a)**, taken from a pixel on the Baltoro tongue, which is denoted by a black circle in panel **(b)**. The unit for all plots is [°C].

TCD
9, 2259–2299, 2015

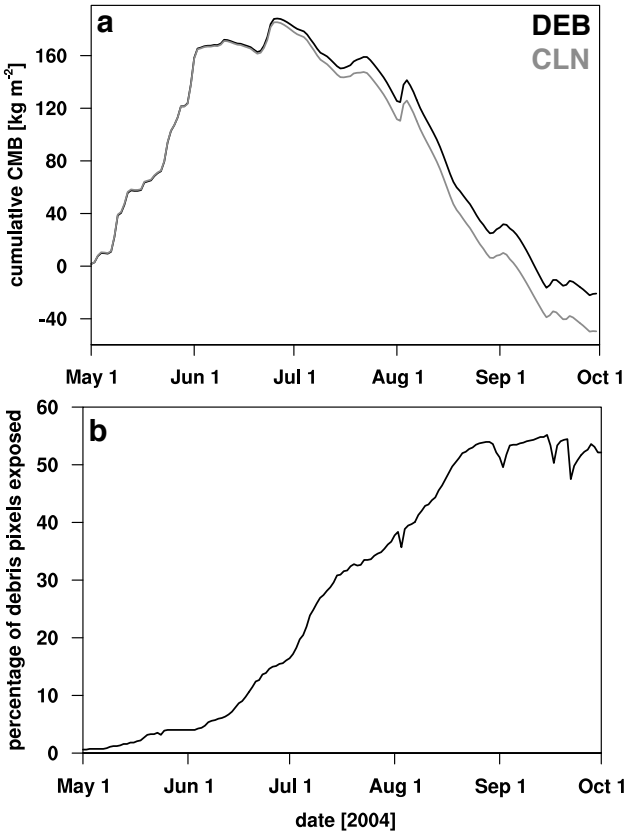

Figure 4. Time series of **(a)** basin-mean cumulative glacier CMB in kg m^{-2} and **(b)** the daily maximum percentage of debris pixels that are exposed in DEB, for DEB (black curve) and CLN (grey) over the whole simulation period of 1 May to 1 October 2004.

TCD
9, 2259–2299, 2015

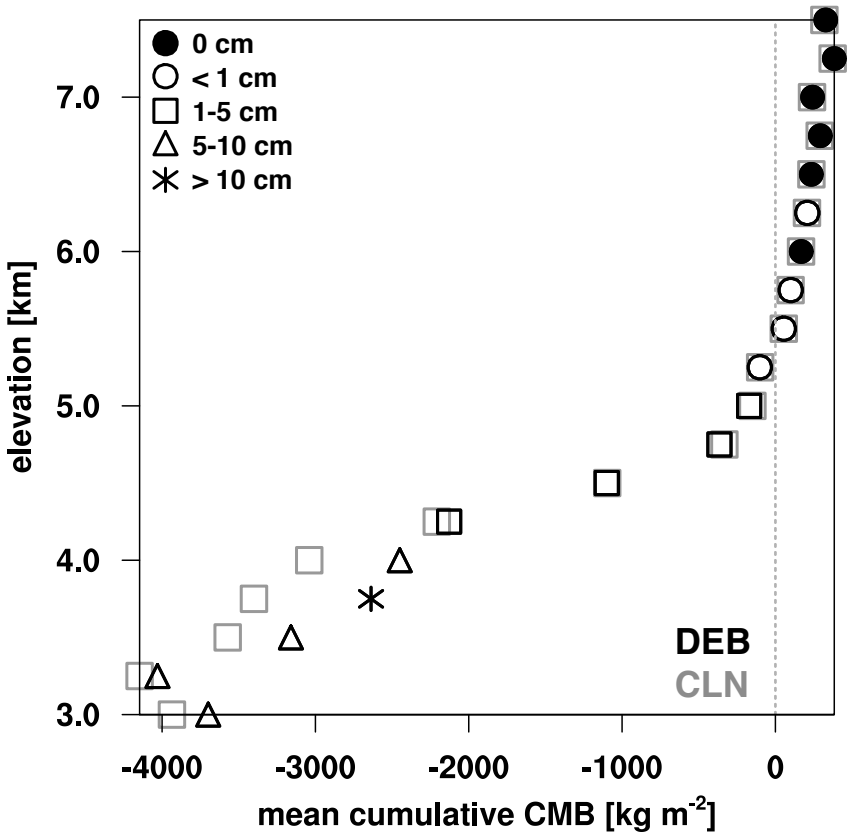

Figure 5. The cumulative vertical balance profile, averaged in 250 m elevation bins between 3000 and 7500 m a.s.l., over all glacier pixels and from 1 July to 1 October 2004. Grey-square markers denote results from the CLN simulation, while those from DEB are plotted with black markers. The shape of the black marker indicates the range of the mean debris thickness in that elevational band.

TCD
9, 2259–2299, 2015

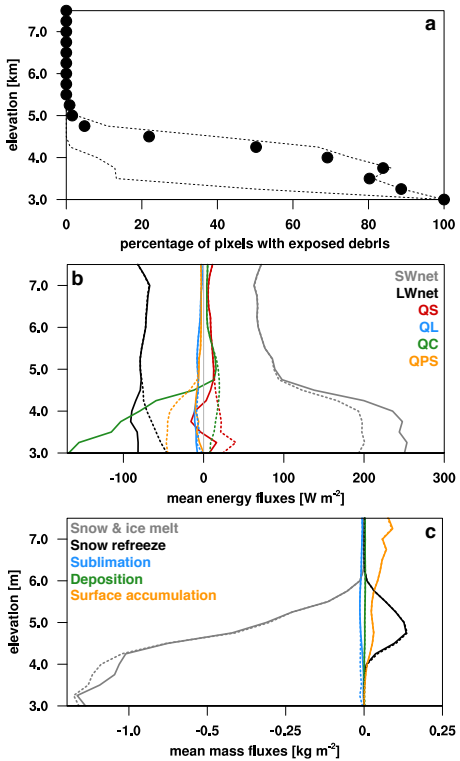

Figure 6. (a) The percentage of debris-covered pixels in each 250 m elevation bin that are exposed on average between 1 July to 1 October 2004. Minimum and maximum values over the same period are indicated by the dashed lines. Elevational profiles of mean glacier **(b)** surface-energy and **(c)** mass fluxes, in units of $W\,m^{-2}$ and $kg\,m^{-2}$ respectively, with the solid (dashed) lines denoting data from DEB (CLN). Note that these profiles correspond to an amalgamation of all glaciated grid cells, rather than the mean elevational profile along glacier.

TCD
9, 2259–2299, 2015

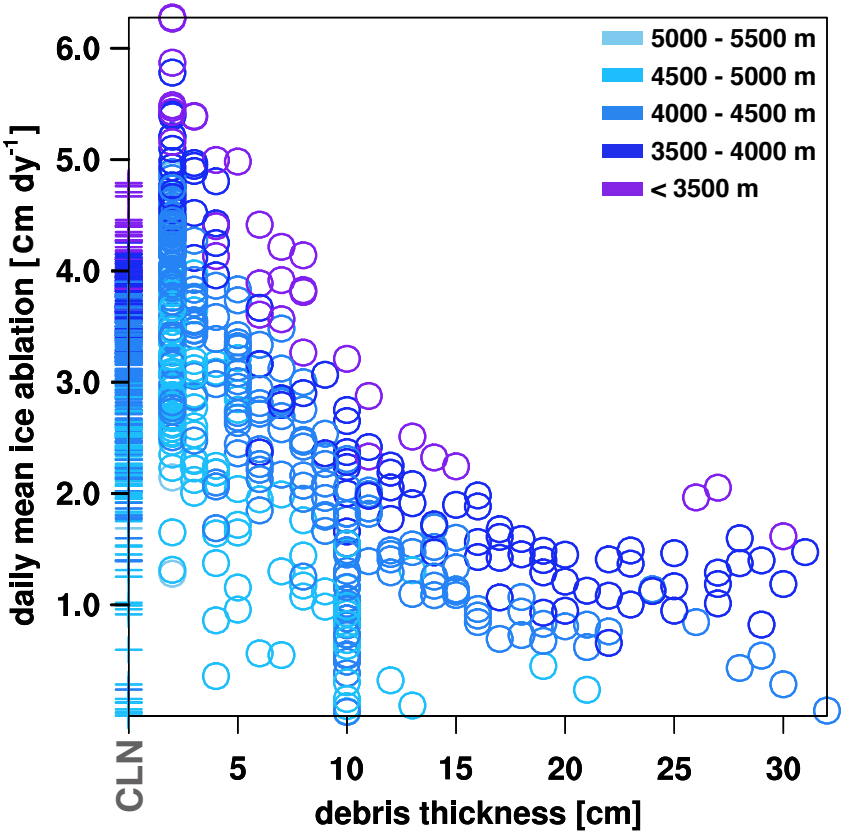

Figure 7. Daily mean ablation rate vs. debris thickness for DEB (circle markers) and CLN (horizontal line markers), with the range of topographic height value of each data point indicated by the color of the marker. Here, "ablation" refers to sub-debris ice melt in DEB (i.e. only snow-free pixels are selected) and total column melt (surface and englacial) in CLN for the same pixels and time periods. The concentration of data points at 10 cm thickness results from the specification of debris where centreline information was unavailable (cf. Sect. 2.3).

TCD
9, 2259–2299, 2015

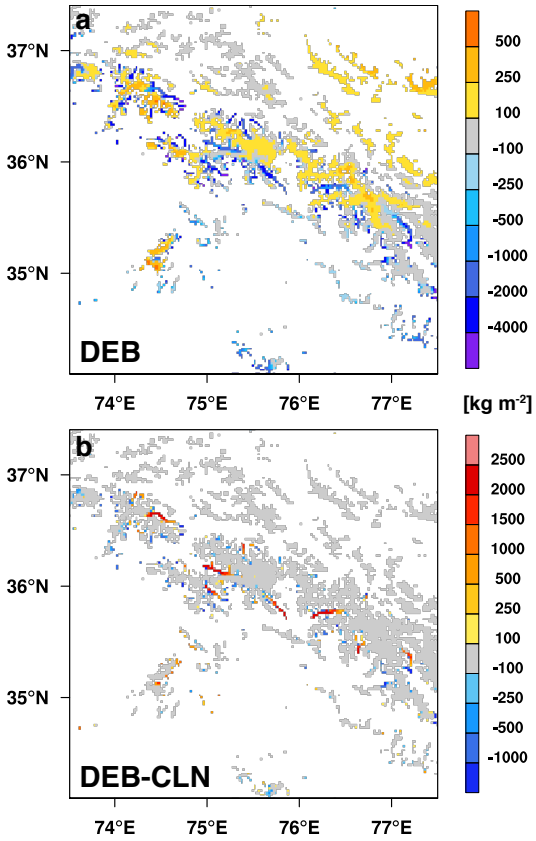

Figure 8. Total accumulated mass balance in [kg m^{-2}] between 1 July and 1 October 2004 for **(a)** the DEB simulation and **(b)** the difference between DEB and CLN.

TCD
9, 2259–2299, 2015

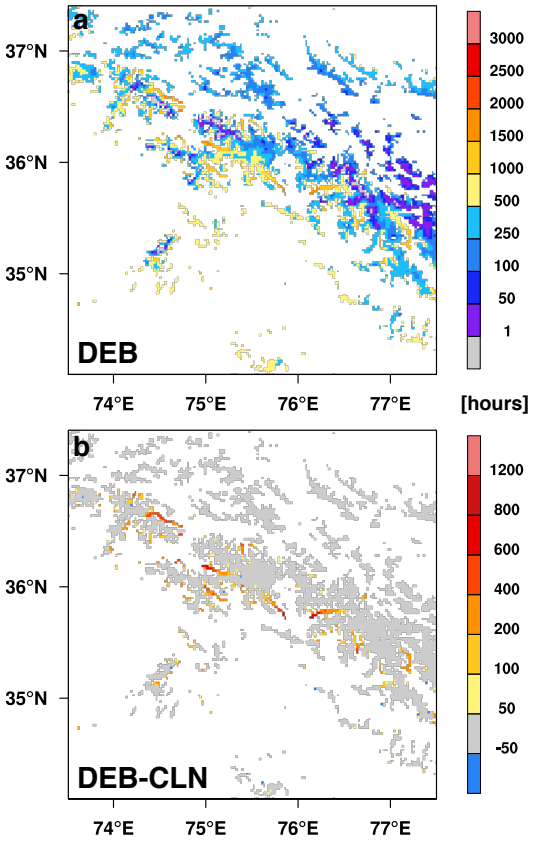

Figure 9. The total number of hours where the surface temperatures reaches or exceeds the melting point "melt hours") for **(a)** the DEB simulation and **(b)** the difference between CLN and DEB.

TCD
9, 2259–2299, 2015

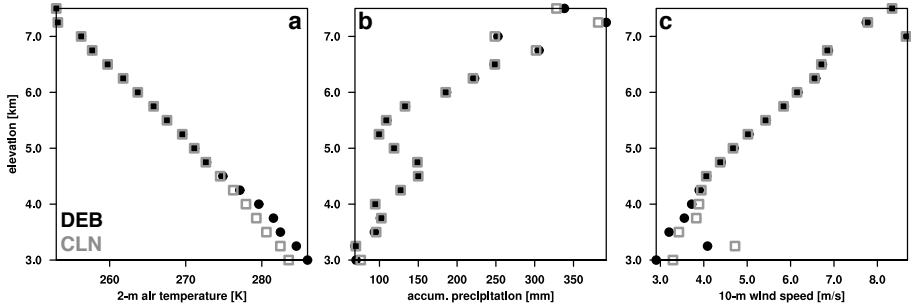

Figure 10. Elevational profiles of near-surface **(a)** air temperature [K] and **(b)** accumulated precipitation [mm], and **(c)** wind speed at a height of 10 m, from the DEB (black-circle markers) and CLN (grey-square) simulations. The temporal period is 1 July to 1 October 2004.

TCD
9, 2259–2299, 2015

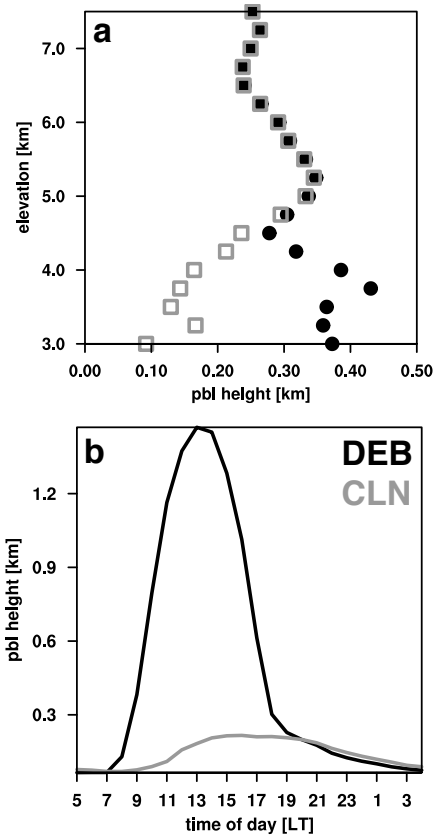

Figure 11. (a) Basin-mean elevational profile and **(b)** diurnal cycle of the planetary boundary layer height over exposed debris in DEB (black markers and curve) and their equivalent pixels in CLN (grey-square markers and curve).

TCD
9, 2259–2299, 2015